Radiofrequency electrode vibration-induced shear wave imaging for tissue modulus estimation: A simulation study (L)

Shyam Bharat and Tomy Varghese[a)]
Department of Medical Physics, University of Wisconsin-Madison, 1111 Highland Avenue, 1159 WIMR, Madison, Wisconsin 53706

(Received 3 December 2009; revised 25 June 2010; accepted 30 June 2010)

Quasi-static electrode displacement elastography, used for *in-vivo* imaging of radiofrequency ablation-induced lesions in abdominal organs such as the liver and kidney, is extended in this paper to dynamic vibrational perturbations of the ablation electrode. Propagation of the resulting shear waves into adjoining regions of tissue can be tracked and the shear wave velocity used to quantify the shear (and thereby Young's) modulus of tissue. The algorithm used utilizes the time-to-peak displacement data (obtained from finite element analyses) to calculate the speed of shear wave propagation in the material. The simulation results presented illustrate the feasibility of estimating the Young's modulus of tissue and is promising for characterizing the stiffness of radio-frequency-ablated thermal lesions and surrounding normal tissue.
 [DOI: 10.1121/1.3466880]

PACS number(s): 43.35.Yb, 43.60.Mn [TDM] Pages: 1582–1585

I. INTRODUCTION

Elasticity imaging has been used in the imaging of coagulated regions created using rf ablative therapies, and *in-vivo* methods include both quasi-static[1,2] and dynamic approaches.[3,4] In quasi-static methods, tissue stiffness is quantified by displaying strain maps of the tissue, while the focus in dynamic methods is usually to detect and track the progress of shear waves resulting from mechanical vibration of tissue. The velocity of the shear waves can be used to determine the shear modulus (and thus, Young's modulus) of tissue. A common example of dynamic elasticity imaging is sonoelasticity imaging, specifically sonoelastography, which uses ultrasound to measure the propagation of shear waves induced by externally-applied mechanical vibrations.[4] Another dynamic method is transient elastography, where a pulsed excitation is coupled into tissue by a piston vibrating perpendicularly to the tissue.[5] An ultrasound transducer placed on the opposite side of the tissue medium tracks the axial component of the transient shear wave. Acoustic radiation force imaging (ARFI)[6] and vibroacoustography[7] are other examples of imaging using dynamic excitation. ARFI utilizes the radiation force of acoustic pulses to perturb tissue directly at the region of interest (ROI). The shear waves generated by the pushing beam pulses are tracked by the tracking beams which are ordinary B-mode imaging pulses directed at a location lateral to the pushing beam pulses. In vibroacoustography, low frequency mechanical excitations (f_{LF}) are generated with the aid of a focused annular array which is used to emit two ultrasound beams at close frequencies f_1 and f_2 ($f_2=f_1+f_{LF}$).

In earlier work, we have discussed the use of the rf ablation electrode as a displacement device, to apply quasi-static minute displacements (on the order of a fraction of a millimeter) to the unconstrained end of the same electrode used to create the thermal lesion.[8,9] In this paper, we extend the concept of quasi-static electrode displacement elastography to monochromatic vibrational perturbations of the rf ablation electrode. The rf electrode is subjected to sinusoidal excitation at low frequencies (1–10 kHz) and an ultrasound transducer placed adjacent to the electrode on the surface of the tissue phantom (similar to the quasi-static case) tracks the resulting shear wave displacements at high frame rates. The velocity of these shear waves can be measured and used to calculate the shear modulus and Young's modulus of both the thermal lesion and the surrounding normal tissue. Shear wave velocity can be measured using various techniques previously described in literature.[4,6,10] The method used in this paper, the time-to-peak (TTP) displacement algorithm, is a time-of-flight measurement technique where the shear wave position is characterized as a function of time.[10]

II. THEORY

A. Shear wave theory

The equation of wave motion in a linear and isotropic medium is given by

$$\frac{E}{2(1+v)}\nabla^2\bar{u}+\frac{E}{2(1+v)(1-2v)}\nabla\nabla\cdot\bar{u}=\rho\frac{\partial^2\bar{u}}{\partial t^2} \quad (1)$$

In the above equation, E is the Young's modulus, ν is the Poisson's ratio, ρ is the density and $\bar{u}$ is the displacement vector. Equation (1) describes the combined wave motion due to longitudinal waves and transverse (shear) waves. Decomposition of this equation into two decoupled wave equations for separately describing longitudinal and shear wave

a)Author to whom correspondence should be addressed. Electronic mail: tvarghese@wisc.edu

 0001-4966/2010/128(4)/1582/4/$25.00

motion has been accomplished earlier.[11] The equation for shear wave motion in a homogeneous medium is shown in Eq. (2).

$$\nabla^2 \overline{u_s} - \frac{1}{v_s^2} \frac{\partial^2 \overline{u_s}}{\partial t^2} = 0 \tag{2}$$

In Eq. (2), $\overline{u_s}$ is the shear wave displacement vector while v_s is the velocity of the shear wave. The shear wave velocity is proportional to the square root of the Young's modulus of the tissue, with the constants of proportionality being the density ρ and the Poisson's ratio ν.

$$v_s = \sqrt{\frac{E}{2\rho(1+\upsilon)}} \tag{3}$$

Since we are concerned with the propagation of shear waves in a nearly incompressible medium ($\nu \sim 0.5$), Eq. (3) simplifies to

$$v_s = \sqrt{\frac{E}{3\rho}} \tag{4}$$

B. Shear wave velocity estimation

The TTP displacement algorithm, a time-of-flight measurement technique, tracks the shear wave propagation in time and relates its space and time progression to calculate the velocity of propagation. The method requires homogeneity of the region over which the estimation process is performed. The TTP displacement method itself involves analysis of displacements over a region lateral to the direction of mechanical excitation, referred to as the region of analysis (ROA). Each pixel is the ROA is temporally analyzed and the time taken to achieve peak displacement is noted, which increases with distance from the region of excitation (ROE). This is intuitive as the shear waves propagate outwards from the ROE. Once this analysis is completed for the entire lateral extent of the ROA, the times-to-peak displacement are plotted against the lateral positions of the pixels corresponding to the respective time delays. The inverse slope of this line is the estimate of the velocity of the shear wave in the ROA.

III. METHODS

A. Finite element analysis

A commercial finite element analysis package, ANSYS (ANSYS Inc., Pittsburgh, PA, USA) was used for modeling the two-dimensional tissue deformation in response to the mechanical stimuli. The model consisted of a cylindrical inclusion (radius 8 mm), with an embedded electrode, centered in a cubic phantom (40 mm × 40 mm × 40 mm). The mechanical properties of the simulated phantom were chosen such that the inclusion-background elastic moduli ratios and the Poisson's ratios match previously published values for liver tissue.[12–14] The electrode was chosen to mimic the Cooltip™ rf ablation system (Valleylab, Boulder, CO), which consists of a single cylindrical electrode with an exposed tip that serves to deposit heat in the tissue. Tissue motion was induced by applying minute sinusoidal displacements (1 kHz, 2 mm peak-to-peak displacement) to the unconstrained end of the rf electrode. The sinusoidal displacement pattern was discretized into a finite number of load steps at a sampling frequency of 20 kHz, thus satisfying the Nyquist criterion. The axial nodal displacements resulting from the vibrational perturbation of the electrode were exported from ANSYS at every load step and subsequently interpolated in a bilinear manner to obtain displacements in a regular 2-D Cartesian matrix format, implemented in MATLAB (The MathWorks, Natick, MA, USA).

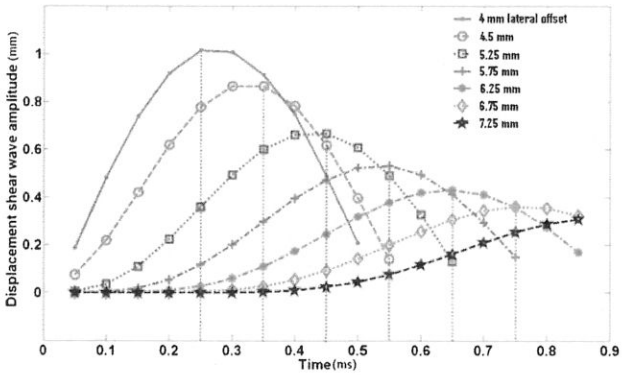

FIG. 1. Temporal progression of the shear wave at different positions in the model lateral to the ROE. Young's modulus of inclusion is 100 kPa.

B. Time-to-peak displacement algorithm

The vibrations imparted to the rf ablation electrode are transferred to the thermal lesion and the surrounding normal tissue, around the vertical region or ROE where the electrode is bound to the thermal lesion. The analysis of shear wave propagation lateral to the ROE is performed, i.e., the displacement at each pixel lateral to the ROE is analyzed over time to track the shear wave propagation patterns. Figure 1 illustrates the shear wave displacement amplitude pattern plotted against time for sinusoidal vibrations at 1 kHz. The shear wave propagation trend is shown here for the region within an inclusion of Young's modulus 100 kPa. The vertical dotted lines in the plots indicate the times at which the pixel at that location reaches its peak displacement value, or TTP displacement. The TTP displacement for each laterally offset pixel (relative to the ROE) is determined and plotted versus the lateral position of the pixel, i.e., distance from the start position. Note that the distance is calculated from the first pixel lateral to the ROE. An example of the relationship between the TTP displacements and the laterally offset distances is shown in Fig. 2. A linear fit is then made to the data and the equation of that line is determined. The inverse slope of the line is an estimate of the velocity of the propagating shear wave. Using the relationship between the Young's modulus and shear wave velocity in Eq. (4), the Young's modulus is calculated for the section of tissue for which the shear wave velocity is estimated. The Young's modulus can be estimated for the thermal lesion as well as surrounding normal tissue. The boundary of the thermal lesion can be determined by the abrupt change in slope of the TTP displacement line plotted against the lateral pixel positions, as

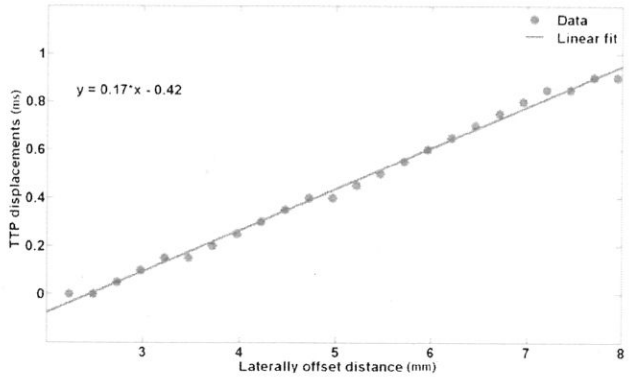

FIG. 2. The TTP displacement of the shear wave at each pixel plotted against the lateral position of that pixel for inclusion modulus of 100 kPa. The inverse slope of this line corresponds to the velocity of the shear wave.

shown in Fig. 3. This change of slope represents the boundary of the inclusion.

IV. RESULTS

This paper presents preliminary results of tracking the propagation of shear waves resulting from periodic sinusoidal vibrations of the rf ablation electrode. The TTP displacements were utilized for estimating the shear wave velocity and thus, the Young's modulus of the thermal lesion and surrounding normal tissue. Table I shows the estimated values of the Young's modulus of the inclusion and background for all the cases studied. The results show good agreement between the estimated and actual values of the Young's modulus for both the inclusion and the background. Since these estimates are based on a finite element simulation, the results are not expected to vary, unless the finite element model itself is changed. Identical perturbations applied to the model would produce the same result as would be expected.

Figure 4 plots the estimated inclusion moduli versus the actual inclusion moduli. It also shows the ideal values plotted as the hyphenated line. The deviation of the estimation curve from this line is a measure of the error in the estimation process. Note that the absolute error in the estimates increases as the modulus of the inclusion increases. Based on this simulation study, we are unclear as to why there is an

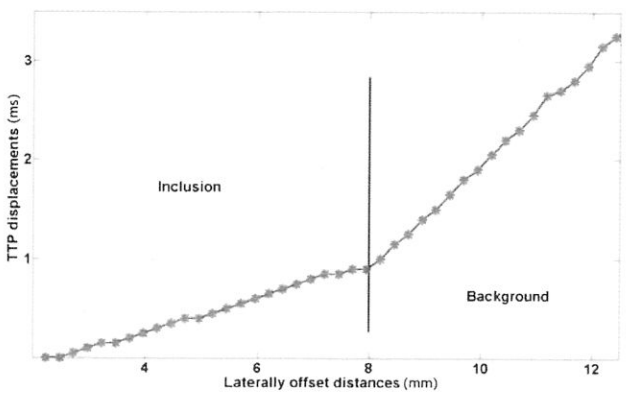

FIG. 3. The change of slope in the TTP displacement line is indicative of the boundary between the inclusion and the background, i.e., a change in the Young's modulus of the underlying propagation medium.

TABLE I. The table presents results from the modulus estimation procedure, for all the different inclusion and background moduli simulated.

Inclusion: background contrast (background 10 kPa)	Estimated inclusion modulus (kPa)	Quality of fit (R^2 coefficient)	Estimated background modulus (kPa)	Quality of fit (R^2 coefficient)
1:1	11.3	0.9831	10.5	0.9975
2:1	26.9	0.881	10.1	0.9999
5:1	57.2	0.9793	8.3	0.9711
10:1	114.1	0.9801	10.5	0.9975

overestimation of the inclusion modulus. It will be interesting to see whether the embedded electrode contributes to this overestimation. Further research using simulations with electrodes of varying stiffness and experimental ultrasound-based modulus imaging studies on tissue-mimicking phantoms is needed to confirm these findings. Also, since the vibrations are first coupled to the inclusion through the rf electrode and then to the background, it will be interesting to study whether the stiffness of the inclusion has any bearing on the estimation accuracy of the modulus of the background.

V. DISCUSSION

In comparison with existing dynamic elasticity techniques, this method conceptually lies between sonoelastography and ARFI. Though the mechanical vibrations are coupled to the tissue using an external device (rf ablation electrode) like in conventional sonoelastography, the excitation is not applied to the tissue surface and does not have to pass through intervening tissue to the ROI. Instead, since the thermal lesion is bound to the electrically-active region of the rf ablation electrode, it ensures that any displacement to the upper unconstrained end of the electrode is transferred directly to the ROI, which in this case is the thermal lesion and immediately surrounding normal untreated tissue. Thus, the net effect is similar to that in ARFI i.e., the ROE coincides with the ROI.

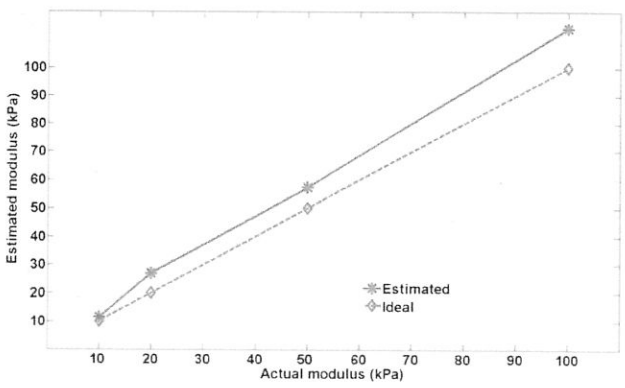

FIG. 4. The estimated inclusion modulus for the different inclusion moduli simulated are plotted against the actual moduli. The bold line represents the estimated values while the dotted line represents the actual values. The deviation of the bold line from the dotted line indicates the errors in the estimation procedure.

The results presented indicate that the Young's modulus of thermal lesions and surrounding normal tissue can be estimated by tracking the propagation of shear waves resulting from vibrating the rf ablation electrode at low frequencies (~1 kHz). The TTP displacement algorithm utilized in this paper provides estimates of the velocity of the propagating shear wave. Note from Eq. (4) that the Young's modulus of the propagating medium is directly proportional to the square of the shear wave velocity. In other words, shear waves propagate faster in stiffer media compared to softer media.

The shear wave propagation pattern in Fig. 3 shows that there is clear change of slope at the interface between two regions of differing stiffness. This could potentially be used as an indicator to demarcate such regions. This transition in TTP displacement slope has been verified to exist for all the modulus contrasts studied in this paper (1:1, 2:1, 5:1 and 10:1). These modulus contrast ratios were chosen based on existing literature on Young's modulus values in the liver and thermally ablated regions created in the liver.[12–14] With regard to monitoring rf-ablated lesions, this method could potentially aid in deciding the boundaries of thermal lesions. The spatial resolution at which the TTP displacements can be estimated is limited by the nodal density of the finite element model. In ultrasound-based displacement imaging, the lateral resolution of the ultrasound scanner and the processing parameters of the displacement estimation algorithm will determine the spatial resolution of the TTP displacement estimation. Additionally, the transition between the lesion and the surrounding normal tissue must occur within the footprint of the ultrasound transducer. In our simulations, we found that the shear wave generated, moves beyond the inclusion into the surrounding background. Since the inclusion is bound to the electrode, it is possible that there will always be some shear introduced into the background due to the movement of the inclusion relative to the background, in which case we expect it to always be possible to detect the boundary of the lesion. Future work will entail studying the propagation of shear waves for different inclusion dimensions to verify if this is indeed true. These are the some of the various factors that could influence the precision of the detected lesion boundaries.

It is also essential to be able to automatically and accurately detect the location corresponding to the change in slope of the TTP displacement curve, prior to estimating the moduli for the different regions. As mentioned earlier, homogeneity of the underlying propagation medium is necessary for accurate estimation of the modulus of that region. Any spatial variations in the modulus of the region where TTP displacement estimation is performed will result in errors in the estimated modulus. To ensure modulus homogeneity, the estimation window size can be reduced. However, reducing the estimation window will lead to fewer data points being used, thus, increasing the noise in the modulus estimated. Thus, there exists a trade-off between the need for homogeneity of the underlying moduli and the need to have more data points for accurate TTP displacement estimation. A detailed study, in which these trade-offs are analyzed and quantified, is warranted. Figure 5 displays the differences in shear wave propagation in inclusions with different moduli. Analyzing the propagation patterns of generated shear waves can provide vital information regarding the stiffness characteristics of the underlying medium.

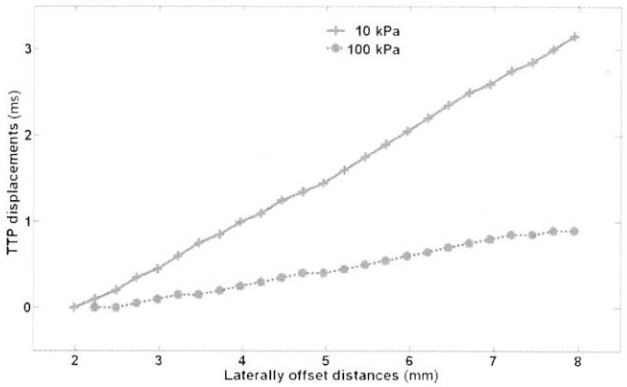

FIG. 5. The TTP displacement trend for image pixels laterally offset from the ROE. The bold curve represents the inclusion with Young's modulus 10 kPa and the dotted curve represents the inclusion with Young's modulus 100 kPa. This figure illustrates that shear wave propagation is faster when the underlying inclusion modulus is higher.

ACKNOWLEDGMENTS

This work was funded by NIH grant R01 CA112192-03, R01 CA112192-04, and R01CA112192-S103.

[1]T. Varghese, "Quasi-static ultrasound elastography," Ultrasound Clin. **4**, 323–338 (2009).
[2]T. Varghese, J. A. Zagzebski, and F. T. Lee, "Elastographic imaging of thermal lesions in the liver in vivo following radiofrequency ablation: Preliminary results," Ultrasound Med. Biol. **28**, 1467–1473 (2002).
[3]B. J. Fahey, R. C. Nelson, S. J. Hsu, D. P. Bradway, D. M. Dumont, and G. E. Trahey, "In vivo guidance and assessment of liver radio-frequency ablation with acoustic radiation force elastography," Ultrasound Med. Biol. **34**, 1590–1603 (2008).
[4]K. Hoyt, B. Castaneda, and K. J. Parker, "Two-dimensional sonoelastographic shear velocity imaging," Ultrasound Med. Biol. **34**, 276–288 (2008).
[5]L. Sandrin, M. Tanter, J. L. Gennisson, S. Catheline, and M. Fink, "Shear elasticity probe for soft tissues with 1-D transient elastography," IEEE Trans. Ultrason. Ferroelectr. Freq. Control **49**, 436–446 (2002).
[6]K. Nightingale, S. A. McAleavey, and G. Trahey, "Shear-wave generation using acoustic radiation force: in vivo and ex vivo results," Ultrasound Med. Biol. **29**, 1715–1723 (2003).
[7]C. Pislaru, B. Kantor, R. R. Kinnick, J. L. Anderson, M. C. Aubry, M. W. Urban, M. Fatemi, and J. F. Greenleaf, "In vivo vibroacoustography of large peripheral arteries," Invest. Radiol. **43**, 243–252 (2008).
[8]S. Bharat and T. Varghese, "Contrast-transfer improvement for electrode displacement elastography," Phys. Med. Biol. **51**, 6403–6418 (2006).
[9]S. Bharat, T. G. Fisher, T. Varghese, T. J. Hall, J. Jiang, E. L. Madsen, J. A. Zagzebski, and F. T. J. Lee, "Three-dimensional electrode displacement elastography using the Siemens C7F2 fourSight four-dimensional ultrasound transducer," Ultrasound Med. Biol. **34**, 1307–1316 (2008).
[10]M. L. Palmeri, M. H. Wang, J. J. Dahl, K. D. Frinkley, and K. R. Nightingale, "Quantifying hepatic shear modulus in vivo using acoustic radiation force," Ultrasound Med. Biol. **34**, 546–558 (2008).
[11]L. D. Landau and E. M. Lifshitz, *Theory of Elasticity* (Elsevier, New York, 1986), Chap. 3, pp. 87–107.
[12]W.-C. Yeh, P.-C. Li, Y.-M. Jeng, H.-C. Hsu, P.-L. Kuo, M.-L. Li, P.-M. Yang, and P. H. Lee, "Elastic modulus measurements of human liver and correlation with pathology," Ultrasound Med. Biol. **28**, 467–474 (2002).
[13]M. Z. Kiss, T. Varghese, and T. J. Hall, "Viscoelastic characterization of *in vitro* canine tissue," Phys. Med. Biol. **49**, 4207–4218 (2004).
[14]S. Y. Emelianov, J. M. Rubin, M. A. Lubinski, A. R. Skovoroda, and M. O'Donnell, *"Elasticity imaging of the liver: Is a hemangioma hard or soft?,"* Proc.-IEEE Ultrason. Symp. **2**, 1749–1752 (1998).